

Who Face Me? Neighbor Identification With LED Camera Communication

JIANHUI ZHANG, TIANHAO ZHANG, FEILONG JIANG AND BEI ZHAO*

*Key Laboratory of Brain Machine Collaborative Intelligence of Zhejiang Province, College of Computer
Science and Technology, Hangzhou Dianzi University, Hangzhou 310018, China*

**Corresponding author: zhaobei@hdu.edu.cn*

Neighbor discovery is a fundamental task to support many other services in wireless multihop networks (WMN). Most existing related methods in WMN rely heavily on the information of radio waves. To extend the way to the neighbor discovery, this paper introduces another interesting way, visual light communication, to explore its property of linear transmission. We apply light emitting diode (LED) array and camera and present a novel communication system, named LED array to camera system (LC). This paper also designs a novel protocol, named LED to camera protocol (LCP), for it. Equipped with an LC, each node in a WMN can determine the precise direction and distance of its neighbors and recognize their identities. Furthermore, this paper also develops a method to infer the topology of the whole network. We design the hardware for LC and conduct extensive experiments to implement the protocol LCP. The average latency of the neighbor discovery is measured and can be as small as 1.087 seconds. LCP can achieve centimeter-level accuracy in distance and direction to averages of 0.37 cm and 1.67 degrees in these real experiments. The relative accuracies in distance and direction measurement are 99.11% and 88.92% on average, respectively. The simulation of the topology inference is also performed to show the feasibility and accuracy with the local distance and direction information.

Keywords: neighbor identification; visible light communication; image processing; topology inference.

Received 29 June 2019; Revised 20 November 2019; Editorial Decision 6 February 2020; Accepted 6 February 2020

Handling editor: Suchi Bhandarkar

1. INTRODUCTION

Wireless multihop network (WMN) has attracted a lot of researches in the past decades [1, 2]. As one of the fundamental tasks, the neighbor discovery arouses a lot of excellent works for its significance in establishing the first contact in the network [3, 4]. Most of the works on neighbor discovery base on the information of the radio wave, which has the properties of diffusion attenuation, refraction, reflection and so on. The properties affect the accuracy of the neighbor discovery. The radio wave may cause a collision when some nodes are working at the same time in the network. Furthermore, the bandwidth of the radio wave is limited and thus valuable resources. These factors motivate us to find another alternative way to discover neighbors.

Fortunately, visible light communication (VLC) brings a desired opportunity because of its linear transmission. It enhances the node to find not only its neighbors but also their distance and direction. There are lots of works on camera/multimedia sensor networks [5]. A few of them

research neighbor discovery with a camera sensor [6], which can find neighbors but cannot confirm their identities with visual light. In this paper, we concern two interesting problems: can the neighbors be found with high accuracy and can their identities be recognized with visual light? The mode of light emitting diode (LED) to camera communication in VLC gives us many inspirations [7, 8]. To apply it, we have to overcome some challenges. Firstly, although the camera can take a picture of the LED, it is hard to determine the distance between them accurately. Secondly, the camera has the character of high energy consumption so it is crucial to decrease the times to use a camera. Thirdly, it is important to transmit data from LED to the camera in an efficient way.

This paper designs a new system LED array to camera system (LC) with an LED array or camera to identify neighbors with high accuracy. To distinguish our work from the traditional radio-based neighbor discovery, this paper introduces a term of *neighbor identification*. In WMN, our LC system cannot only measure the distance and angle between a node and its neighbors but also obtain their identities with visual light. LC

can provide a one-to-many type of neighbor identification. It can also obtain the structure characteristic of the network, such as topology, by the distributively accurate measurement of the distance and angle among nodes. Certainly, the application scenarios of our LC system are not limited to the WMN. LC provides a way of light-based identification that enables the discovery and interaction among different objects. For example, it can be applied to the recognition and information interaction between robots or intelligent cars. Besides, based on LC, we may further realize a way of light communication where data transmission can still take place with some relay nodes when the LED is not captured by the camera. We design a protocol LED camera to protocol (LCP) to support LC. In addition to the system design and performance evaluation, we study LC's application in topology inference. We also perform extensive simulations to validate its feasibility.

The contributions of this paper are listed below:

- Combined with VLC, this paper presents a novel system LC to provide a new way to identify neighbors.
- LC eliminates ambiguities in expressing identities by designing a special LED array pattern. With the well-designed protocol LCP, it can achieve the correct expression and extraction of identities.
- With the distributive neighbor identification, this paper proposes a method to infer the topology of the whole network. We also perform extensive simulations to verify the feasibility of constructing network topology through neighbor identification. The simulation results show that a 90% similar topology can be constructed with only six identification processes when there are 120 nodes deployed in the network.
- We build a testbed of LC and conduct experiments in an indoor environment. The results demonstrate that LC has at least 70% identification accuracy under various conditions. The average identification latency is as small as 1.087 seconds. The average errors are 0.37 cm and 1.67° on the distance and angle measurement, respectively. The relative average errors on them are 0.89% and 11.08%, respectively.

Roud Map. After motivation illustration and challenge explanation in Section 2, Sections 3 and 4 describe system design and details of protocol (LCP), respectively. Section 5 presents the inference process of topology construction. Sections 6 and 7 provide experimental evaluation and simulation results, respectively. Section 8 introduces related work and Section 9 concludes this paper.

Most symbols in this paper are summarized in Table 1.

2. MOTIVATION AND CHALLENGE

2.1. Motivation

Neighbor discovery is a fundamental technique in WMN since it serves as a critical step to establish communication in the

TABLE 1 Symbol and meaning.

Sym.	Description	Sym.	Description
v	Node	l	LED
I	Node ID	d	Distance of LEDs
P	Temporary ID pair	m	# of LEDs
t	Value in P	k	# of nodes
b	Binary value of t	n	# of zero bits
S	Set of LED positions	(x, y)	Coordinate of LED
G	Group of coordinates	R	Communication radius
N	Set of $2^i, i = 0, \dots, n$	T	Registration frame period

network [4, 9–11]. Most of the existing works on neighbor discovery are based on the information of radio waves [3, 12]. For example, the information from radio waves, such as received signal strength (RSS), is adopted to locate the nodes' positions [13, 14]. Radio wave has the inherent properties of diffusion attenuation, refraction, reflection and so on, which may be timevariable [15]. So the node in WMN can merely determine the neighbor nodes in its communication range and their rough distances. The neighbors' positions can be estimated only after some algorithms, such as the three-step localization algorithm in [16], are adopted to exchange the related information among nodes. In another case, the node is equipped with the directional antenna and the estimation accuracy for the neighbor direction can be improved. But it is still rough and the distance estimation among nodes is not improved. The cooperation among nodes is still needed [17].

Furthermore, a successful neighbor discovery can take place when a node listens on the channel and at the same time another one sends a beacon [18]. Thus, an intricate protocol is required to ensure its upper-bounded latency. However, they suffer performance degradation when a large number of nodes deployed in the network mainly due to the existence of channel conflicts. On the other side, this kind of neighbor discovery can only identify nodes within communication range and cannot determine their exact relative positions. Although some works realize node localization, many of them involve complex signal processing inevitably, thus resulting in non-ignorable overhead on limited energy budgets since antenna consumes most of the energy when it works [19–21].

In recent years, VLC becomes a research hot topic and it has the good property: linear transmission. In many VLC works, the LED as a light source is introduced due to its properties of low power consumption and supporting high flashing frequency. Besides, the appearance of small low-cost and low-power camera sensor provides a boost to the VLC research, which provides an opportunity to obtain the light information of LED without loss the sharpness [6, 22]. Therefore, we explore a new paradigm that applies the communication mode in VLC to WMN to realize neighbor identification. There are two desirable advantages: (i) Change in light intensity can be

primely captured by the camera sensor and (ii) modulating light with a specific meaning makes the node in an energy-efficient state.

2.2. Challenges to adopt VLC

In the mode of the LED to camera communication, the LED transmits data by flashing at a high frequency and meanwhile the camera captures consecutive pictures [23]. Due to the rolling shutter effect of CMOS camera, the light signals appear in the picture as stripes with different colors [7]. By detecting the colors of these stripes, the data carried by the light signals can be obtained. Usually, OpenCV is a common tool for image processing. For example, Yang *et al.* and Hao *et al.* adopt OpenCV to extract the region of light in the picture and further recognize each stripe [8, 24]. Finally, a bit string can be obtained from each picture. Although the purpose of these VLC works is different from our LC system, the existing methods of expressing data by flashing LEDs and extracting data from pictures can be used for reference. We apply this communication mode to our LC system in which the node equipped with a camera sensor is called *observer* and the node equipped with three LEDs is called *actor*. Two practical challenges we face are elaborated below.

2.2.1. Ambiguities in identity expression

Thanks to the employment of the camera sensor, the observer node is able to obtain the image information of surrounding actor nodes, which are equipped with an LED array. However, these actor nodes are usually deployed randomly in real applications. Their different locations and orientations make it possible for the observer node to extract identities incorrectly. In order to realize the correct extraction of identity from the picture, the pattern of the LED array is of great significance. An unsatisfactory LED array pattern may cause ambiguities in identity expression.

Figure 1 shows three example scenarios where an imperfect LED array pattern causes a problematic identity extraction. We let the actor node turn on certain LEDs to express its identity and the observer node extract identity from the picture taken. Specifically, the observer node needs to detect the LEDs from the picture and then figures out what it means. In Fig. 1, we use a solid circle to indicate an on LED and a hollow circle to indicate an off LED. The first one, in Fig. 1a, shows that an actor node turns all three LEDs on. However, the observer node cannot determine whether it is upside down even if three LED positions can be all detected. The example in Fig. 1b shows that there is a confusion of two possible LED array positions so that the observer node cannot determine the true message expressed by the actor node. Moreover, due to the uncertain distance between the observer node and the actor node, there is also a scenario as shown in Fig. 1c. An off LED may be in the middle of two on LEDs. These ambiguities arise due to the uncertainty among LED positions. Therefore, a proper LED

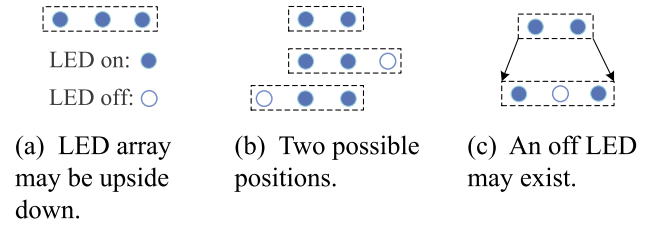


FIGURE 1. Imperfect LED array cannot express message correctly.

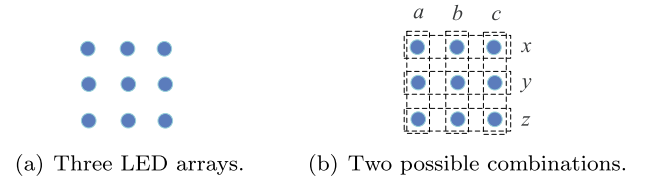


FIGURE 2. The difficulty to distinguish multiple LED arrays.

array pattern is an urge to be designed to ensure LED array can be highly detectable, especially when multiple actor nodes present different positions and orientations.

Additionally, a message expression method based on LED array shall be designed elaborately. Two conditions should be satisfied: (i) ensuring the observer node can detect all LED positions from the picture and (ii) guaranteeing the uniqueness of the message expressed by each actor node.

2.2.2. Interference in identity extraction

The second challenge is to deal with interference among multiple LED arrays. When more than one actor nodes locate together, multiple LED arrays appear in the field of view (FoV) of the camera. Light beams from one LED array affect that from another one inevitably.

Figure 2a gives an example where three actor nodes are adjacent in positions. At this point, the observer node cannot determine which is the true combination. Specifically, the observer node cannot distinguish whether the horizontal three LEDs come from the same actor node or vertical three ones, as shown in Fig. 2b. Also, the actual exhibition of the LED array may not ideally be a horizontal or vertical line. Three LEDs may on an oblique line and with different compactness in the picture. To overcome this challenge, an algorithm that exploits the features of the LED array is developed, which is robust against different rotation angles of actor nodes.

3. SYSTEM DESIGN

3.1. Design overview

As mentioned before, our system equips each node with a camera sensor and three LEDs. These three LEDs form a

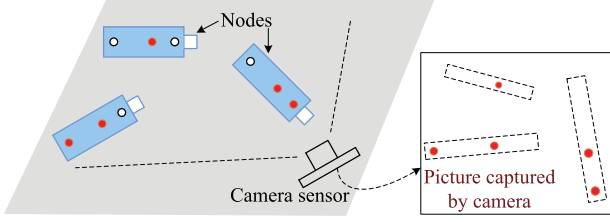


FIGURE 3. System overview of LC.

special LED array as they are arranged in particular positions. Besides, each node is assigned a unique ID, denoted by I , beforehand and can communicate with other nodes through a built-in omnidirectional antenna. Figure 3 illustrates the system overview of LC. Multiple actor nodes express their own identities via three LEDs. Meanwhile, an observer node equipped with a camera sensor takes a picture of these actor nodes. Applying a simple image processing method, each on LED, in the picture can be easily detected. Then the observer node can derive these actor nodes' identities by exploiting these LED positions. Finally, neighbor identification is realized. We leave details to the later sections.

The design of LC consists of three components. The first one is identity expression. In this component, we introduce a special pattern of the LED array in detail. Also, a basic identity expression method based on the LED array is presented. The second component is identity extraction in which an image processing method used to detect LED is described. We also analyze some potential problems when the basic identity expression method is applied directly. To solve these problems, we design the LCP in the third component. Specifically, LCP gives an advanced identity expression method and provides a multi-node identification (MI) algorithm. The method of measuring neighbors' relative distances and angles is also described. We put the first two components in this section and the third component in Section 4.

The technique steps proposed in later sections can be summarized in Fig. 4.

3.2. Expressing identity with LEDs

As previously discussed, there are some undesired scenarios when expressing the identity via the LED array. Thus, a special LED array pattern is designed in our LC system. It can ease LED array detection even when the actor node presents various positions and orientations relative to the observer node.

3.2.1. LED array pattern

The LED array pattern refers to a special positional relationship of three LEDs. Three LEDs are arranged with heterogeneous spacing in a straight line. Figure 6 shows an example, i.e. TelosB node with LED arrangement. We illustrate the LED

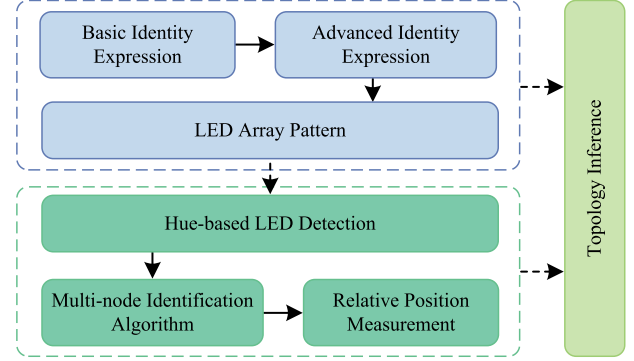
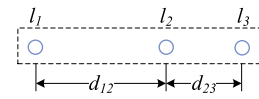


FIGURE 4. Flowchart of LC system.



One LED array: l_1, l_2, l_3

FIGURE 5. LED array pattern.

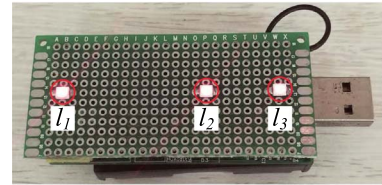


FIGURE 6. TelosB node with arranged LEDs.

array pattern in Fig. 5. An LED array incorporates three LEDs: l_1, l_2 and l_3 , where l_1 is defined as the highest position in the array and l_3 represents the lowest position. Let d_{12} and d_{23} denote distances between l_1 and l_2 , and l_2 and l_3 , respectively. The distance d_{12} is set to be twice of the distance d_{23} , i.e. $d_{12} = 2d_{23}$.

This special pattern design provides two benefits in our LC system. First, the observer node can determine the highest and lowest positions of the LED array even if the actor node is upside down because the ratio of d_{12}/d_{23} is always a constant. Second, if multiple actor nodes appear in the FoV of camera, such design also serves as a criterion for determining which three LEDs come from the same actor node as illustrated in Section 4.3.

3.2.2. Basic identity expression method

To express identity with an LED array, LC adopts a basic identity expression method. The actor node transmits a short message at a time and each short message is determined by the status of the LED array. Denote the number of LEDs in an array

pattern by m . In our system, $m = 3$. We specify that each LED represents one bit as each one can work in two states: *on* and *off*. The bit is 1 when the LED is on and 0 otherwise. The short message transmitted via LED array is actually a binary value of the actor node's identity and contains m bits. So one LED array can express the identity from 0 to $2^m - 1$. For example, if an actor node's ID equals 2, i.e. $I = 2$, then its binary value is 010. It can turn on l_2 and turn off l_1 and l_3 to express its identity.

3.3. Extracting identity from the picture

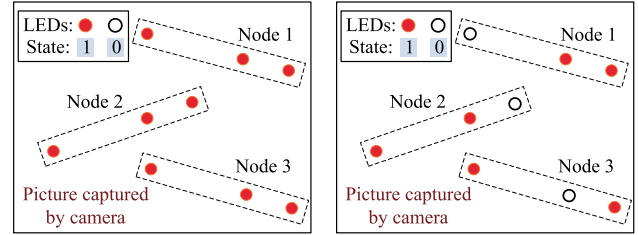
3.3.1. Hue-based object detection

After multiple actor nodes express their own identities via LED arrays, the observer node turns on the camera sensor to take a picture. This picture contains the status of every LED array that appears in the FoV of camera sensor. Each on LED in the picture can be detected according to its color of emitted light beams. In our LC system, the LED emits a red light beam when it is turned on. Thus, an on LED appears as a red region in the picture. The observer node applies a hue-based object detection method to detect red objects in this picture. The hue-based object detection is a lightweight method that calculates hue and saturation of each pixel of the object and then uses them as the primary filtering parameters [25, 26]. Specifically, the observer node converts the Red Green Blue (RGB) images to an Hue Saturation Value (HSV) image and then filters out pixels whose hue and saturation are not within our desired value range. With this method, all on LEDs in the picture can be detected. LC records all LED positions into a set S and further uses the set S to determine each actor node's identity.

3.3.2. Analysis

However, it may be infeasible to determine each actor node's identity with only a set S . There are two conditions we have to satisfy as mentioned before: (i) an observer node must detect all LED positions from the picture so that it can perform grouping operation, i.e. determining which three LED positions come from the same LED array. There must be $k * m$ LED positions in the set S , where k denotes the number of actor nodes that appeared in the FoV of camera sensor. (ii) The identity expressed by each actor node shall be different from each other so that the observer node can distinguish them.

To satisfy the first condition, all LEDs of each actor node are required to be turned on. The picture taken at this time is shown in Fig. 7a. The observer node can obtain all LED positions and then get them grouped. Whereas, these actor nodes cannot be distinguished from each other due to the same identity, i.e. the same LED array state. Figure 7b indicates the case where each actor node expresses a different identity. Nevertheless, the observer node cannot extract identities correctly, because the set S contains only positions of on LEDs. The grouping operation cannot be performed. Hence, the two conditions above cannot be satisfied simultaneously. The main reason is that the hue-based detection method can only detect on LED,



(a) All actor nodes express the same identity. (b) Each actor node shows different identities.

FIGURE 7. Cannot satisfy both conditions at the same time.

thus limiting observer node's ability to determine which array pattern an LED belongs to.

To remove this limitation, we design LCP in the next section. It gives an advanced identity expression method that works for two rounds. With this method, those actor nodes express their identities twice and the observer node takes the picture twice as well. For each picture, the hue-based object detection method is applied. Consequently, the observer node obtains two sets: S_1 and S_2 .

4. LED TO CAMERA PROTOCOL

In this section, we elaborate LCP that gives an advanced identity expression method to enhance the ability of the observer node to perform a grouping operation. This advanced method is a way for actor nodes to express identities in two rounds. Furthermore, LCP provides the MI algorithm for the observer node to extract multiple identities from two pictures. Additionally, LCP gives a method of measuring neighbors' relative distances and angles.

4.1. Registration phase

For the purpose of neighbor identification, we need to match the identities extracted from the picture with nodes' IDs. Thus, there is a preparatory phase for an observer node to collect all actor nodes' IDs. In this phase, each actor node sends a radio frame to the observer node to register its ID. We call this radio frame the *registration frame* for it contains only the actor node's ID in its payload. So its transmission and reception do not involve complex signal processing. Meanwhile, the observer node maintains a *neighbor table* to record each actor node's ID.

Figure 8 shows an example. An observer node v_i has a circular communication range with radius R . The FoV of camera sensor it equipped is depicted by a sector. Four actor nodes locating in the communication range send registration frames separately. When an observer node v_i receives these registration frames, it extracts each one's ID and inserts a corresponding entry into the neighbor table.

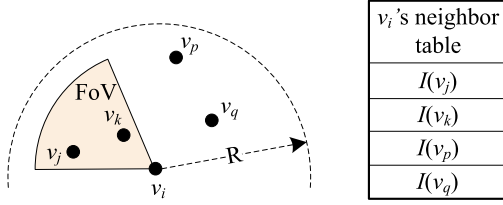


FIGURE 8. The observer node v_i collects four actor nodes' IDs.

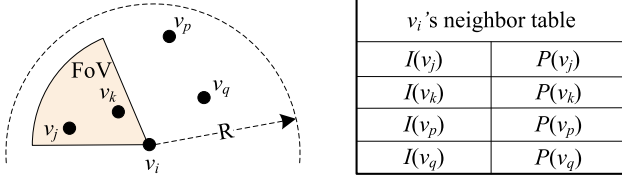


FIGURE 9. The observer node v_i updates neighbor table with temporary ID pairs.

In reality, the preparatory phase may be omitted if the observer node can obtain such adjacency information from other applications.

4.2. Advanced identity expression method

Due to the limitation of basic identity expression method, LCP gives an advanced identity expression method. It is applied by the observer node when all actor nodes' IDs are recorded. At this point, the neighbor table is updated with additional information, i.e. temporary ID pair denoted by P . As shown in Fig. 9, the neighbor table matches each actor node's ID to its temporary ID pair. Each temporary ID pair contains two values and is subsequently assigned to the actor node by wireless communication. In the description of LCP, the term identity always refers to the temporary ID pair.

When actor nodes are assigned with such temporary ID pairs, they express these new identities through their LED arrays in two rounds. The temporary ID pair is denoted by $P = [t_1, t_2]$ where t_1 is a value in the range of $0, \dots, 2^m - 1$. The second value t_2 is determined by the complement operation.

DEFINITION 4.1. (Complement operation). Denote t_1 's binary complement by \bar{t}_1 . Let n denote the number of zero bits in \bar{t}_1 . Then set $N = \{0, \dots, 2^n - 1\}$ is obtained. Each element in N is converted to a binary value and then inserted to the zero position of \bar{t}_1 's bits from right to left. The obtained binary value is denoted by t_2 . Then observer node assigns the same value t_1 and different t_2 to 2^n actor nodes.

Again take Fig. 8 as an example where an observer node v_i has four actor nodes: v_j, v_k, v_p and v_q . To generate an adequate number of temporary ID pairs, node v_i sets $t_1 = 5$ for all actor

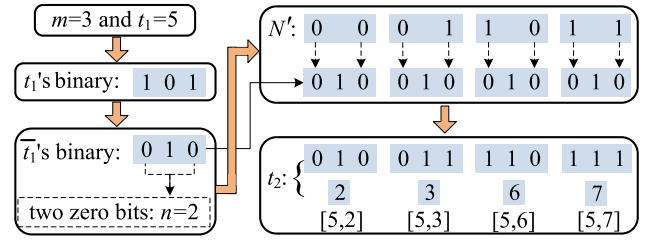


FIGURE 10. The example of the complement operation.

TABLE 2 All possible temporary ID pairs when $m = 3$.

No.	t_1	t_2
0	000	111
1	001	110,111
2	010	101,111
3	011	100,101,110,111
4	100	011,111
5	101	010,011,110,111
6	110	001,011,101,111
7	111	000,001,010,011,100,101,110,111

nodes. Since t_1 's binary value is 101, its binary complement is 010. There are two zero bits in 010, i.e. $n = 2$. Then set $N = \{0, 1, 2, 3\}$ is obtained. Convert each element in N to a binary value. Then set $N' = \{00, 01, 10, 11\}$ is obtained. Each element in N' is inserted into the zero position of 010. The second value t_2 for v_j is 010, for v_k is 011, for v_p is 110 and for v_q is 111. The process is summarized in Fig. 10. Finally, four actor nodes are assigned with temporary ID pair $[5,2]$, $[5,3]$, $[5,6]$ and $[5,7]$, respectively.

By the complement operation, all temporary ID pairs can be worked out. Table 2 lists all available temporary ID pairs when $m = 3$.

To illustrate the applicability of this advanced identity expression method in our work, we are ready to introduce a useful property, which enables the observer node to distinguish each actor node.

PROPERTY 4.1. b_1 and b_2 are the binary values of temporary ID pair's first and second values, respectively. The result of b_1 OR b_2 always is the maximum value that an actor node can express, i.e. $2^m - 1$.

The verification of Property 4.1 is straightforward as b_2 is equal to the binary value of \bar{t}_1 plusing several bits at zero positions. With Property 4.1, the observer node is able to obtain all three LED positions in arbitrary identity expression as long as the temporary ID pair is generated by complement operation.

For example, an actor node v_k is assigned a temporary ID pair $[5, 3]$, the binary values of t_1 and t_2 are $b_1 = 101$ and $b_2 = 011$, respectively. By expressing this identity through its LED array, the observer node can get a set S_1 containing LED

array's highest and lowest positions in the first round, and a set S_2 containing middle and lowest positions in the second round. Finally, all three LED positions can be obtained, i.e. $S = S_1 \cup S_2$.

In general, the advanced identity expression method is very suitable for our work. It well satisfies the demand of getting all LED positions obtained by observer node while keeping the uniqueness of each identity. Compared with the basic identity expression method mentioned above, the advanced identity expression method has more scalability. Theoretically, when $m = 3$, it can be applied to a situation where an observer node has no more than eight actor nodes.

4.3. Multi-node identification algorithm

With the application of advanced identity expression method, the whole neighbor identification process works in two rounds. The observer node obtains two pictures of actor nodes. For each picture, the hue-based object detection method is applied to detect on LEDs. Then sets S_1 , S_2 and S are obtained where $S = S_1 \cup S_2$ contains $k * m$ LED positions. With S_1 , S_2 and S , observer nodes are now able to extract identities by analyzing these LED positions.

When more than one actor nodes appear in the FoV of camera sensor, the observer node firstly divides the set S into several groups. This grouping operation benefits from the LED array pattern designed in section 3.2.1. Specifically, in the picture captured by camera sensor, the Euclidean distances among three LEDs (d_{12} and d_{23}) may be different from other node's ones. The ratio of them certainly satisfies the condition for any actor node, i.e. $d_{12}/d_{23} = 2$. Denote three LED positions picked from set S by three coordinates (x_1, y_1) , (x_2, y_2) and (x_3, y_3) . If they come from the same LED array, we have two following equations:

$$\frac{y_2 - y_1}{y_3 - y_1} = \frac{y_3 - y_1}{y_2 - y_1} \quad (1)$$

$$\frac{x_2 - x_1}{x_3 - x_1} = \frac{y_2 - y_1}{y_3 - y_1} \quad (2)$$

By these two equations, LC can check and group LED positions in set S . Each group containing three LED positions represents an LED array. For each group, LED positions in the sets S_1 and S_2 that belong to the same LED array can be picked out. That is, LC is able to determine which LEDs that actor node turns on at both time when a picture is captured. Thus observer node can figure out the messages that actor nodes expressed in each round and get each one's identity, i.e. temporary ID pair.

For example, a group contains three coordinates denoted by G and $G = \{(155, 44), (219, 46), (251, 47)\}$. These three coordinates are the highest, middle and lowest position in an LED array pattern, respectively. The observer node then searches the LED positions that belong to group G in two sets, S_1 and S_2 . There are two LED positions in set S_1 and two in set S_2 that belong to G , which are denoted by $G_1 = \{(155, 44), (251, 47)\}$

and $G_2 = \{(219, 46), (251, 47)\}$, respectively. So it can get binary value 101 that actor node expressed in the first round and 011 in the second round, thus getting temporary ID pair [5, 3]. Finally, the observer node searches an entry where the temporary ID pairs equal [5, 3] in its neighbor table and know which node it faces.

After one neighbor node gets identified, LC repeats the same procedure to remaining LED positions of three sets until all neighbors get identified. Our MI algorithm is listed in Algorithm 1.

ALGORITHM 1 THE MI ALGORITHM

- **Input:** S_1, S_2, S
- **Output:** Node ID list J
- 1: $G \leftarrow \phi, G_1 \leftarrow \phi, G_2 \leftarrow \phi;$
- 2: **while** $S \neq \phi$ **do**
- 3: **repeat**
- 4: Select three elements e_1, e_2, e_3 from S ;
- 5: **until** e_1, e_2, e_3 satisfy both Equation 1 and 2
- 6: $G \leftarrow G \cup \{e_1, e_2, e_3\};$
- 7: **for** each element e in S_1 and $e \in G$ **do**
- 8: $G_1 \leftarrow G_1 \cup \{e\};$
- 9: **end for**
- 10: **for** each element e in S_2 and $e \in G$ **do**
- 11: $G_2 \leftarrow G_2 \cup \{e\};$
- 12: **end for**
- 13: Determine node ID I and insert I to the J
- 14: $S \leftarrow S - G, S_1 \leftarrow S_1 - G_1, S_2 \leftarrow S_2 - G_2;$
- 15: $G \leftarrow \phi, G_1 \leftarrow \phi, G_2 \leftarrow \phi;$
- 16: **end while**
- 17: **return** J ;

4.4. Measurement of relative position

Besides the extraction of identities from the picture, the determination of neighbors' relative positions can also be achieved. By exploiting the imaging mechanism of convex lens, the observer node can calculate actor nodes' relative distances and angles [6, 27]. Figure 11 shows the imaging process of the camera. O denotes the camera lens. The orientation of camera can be denoted by a vector \vec{OL} . L' is a projection of L on the image plane, which is also a center of the captured picture.

A line segment RK represents an LED array on the node where R and K denote LED l_1 and l_3 , respectively, as mentioned in Fig. 5. The middle of R and K is denoted by Q . The projections of these three points are denoted by R' , Q' and K' , respectively. The camera maintains a coordinate system for its captured picture. Thus, every point has a pair of coordinates for its unique position on the image plane. L' has a coordinate of $(0, 0)$ since it is a center of the picture. Likewise, the coordinates of R' , Q' and K' are denoted by $(x_{R'}, y_{R'})$, $(x_{Q'}, y_{Q'})$ and $(x_{K'}, y_{K'})$, respectively. By measuring the number of pixels,

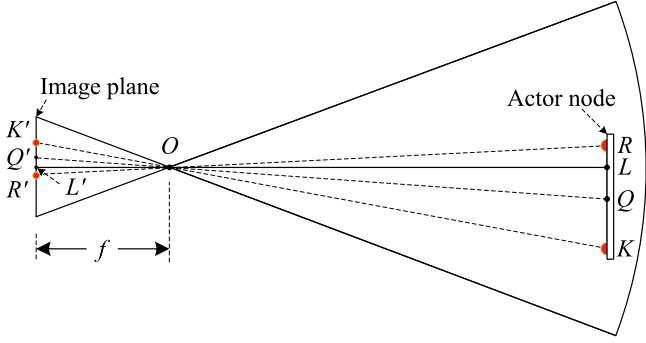


FIGURE 11. An actor node and its projection on the image plane.

we have

$$|R'K'| = \sqrt{(x_{R'} - x_{K'})^2 + (y_{R'} - y_{K'})^2}. \quad (3)$$

$$|L'Q'| = \sqrt{x_{Q'}^2 + y_{Q'}^2}. \quad (4)$$

Based on the imaging mechanism, we get two pairs of similar triangles: $\triangle R'K'O \sim \triangle RKO$ and $\triangle L'Q'O \sim \triangle LQO$. In the first pair of similar triangles, we have

$$\frac{|R'K'|}{|L'O|} = \frac{|RK|}{|LO|}. \quad (5)$$

Note that $|L'O|$ is the focal length of the camera and we denote such a known parameter by f . The length of line segment RK is also a constant that can be measured in advance and we let $|RK| = C$. So the vertical distance between node and camera can be obtained as

$$|LO| = \frac{|RK| \cdot |L'O|}{|R'K'|} = \frac{C \cdot f}{|R'K'|}. \quad (6)$$

Similarly, in the second pair of similar triangles, we have

$$|LQ| = \frac{|L'Q'| \cdot |LO|}{f} = \frac{C \cdot |L'Q'|}{|R'K'|}. \quad (7)$$

Then the distance and angle of the node relative to the camera can be calculated as

$$|QO| = \sqrt{|LO|^2 + |LQ|^2}, \quad (8)$$

$$\angle LOQ = \arctan\left(\frac{|LQ|}{|LO|}\right).$$

If the node is not facing forward to the camera, the $\triangle LQO$ is a right triangle no more. So the Pythagorean theorem is no longer suitable for the calculation of the length of line segment QO . Nevertheless, the real distance between two nodes in the network is usually much greater than the size of the node

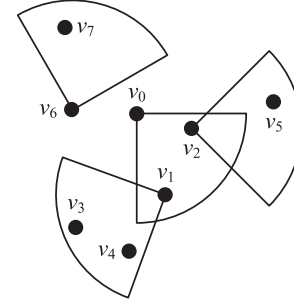


FIGURE 12. The example of WMN.

itself, i.e. $|LO| \gg |RK|$. In this case, when node's orientation changes, the variation of $\angle LOQ$ is merely within a small range. At this point, if the Pythagorean theorem is still used to the calculation, the measurement error might increase a little bit but we believe that it is within an acceptable limit.

5. TOPOLOGY INFERENCE

In this section, we illustrate a practical application of neighbor identification, i.e. topology inference. Understanding the network structure is of great significance for network management and resource deployment. Compared with the neighbor discovery by wireless communication, the way to identify neighbors through image is much accurate and faster because there is no such problem as channel conflict. Such image-based method can inherently provide a one-to-many type of identification. Thus, it has good performance in terms of time.

Figure 12 depicts a simple example of WMN in which eight nodes are deployed randomly. Each node's radio coverage area can be represented by a circle with radius R . Two nodes with a distance less than R can communicate with each other and transmit/receive neighbor identification information. The sector represents the FoV coverage area of camera sensor equipped on each node. Each node can identify neighbors locating in its sector. For the sake of clarity, we draw only the fan-shaped coverage area of each node.

Among them, one node plays a special role. Node v_0 serves as a sink node. The sink node collects all available identification information and subsequently reduces network topology layer by layer, as shown in Fig. 13. Specifically, the sink node is recorded in the first layer. Those nodes identified by sink node and not present in the previous layer are recorded in the next layer. If a node does not appear in the neighbor identification chain of sink node but there is a communication path between them, then it is recorded in the first layer. Then nodes of subsequent layers are obtained in the same way until there are no available nodes. Thus, a directed graph describing network topology can be obtained.

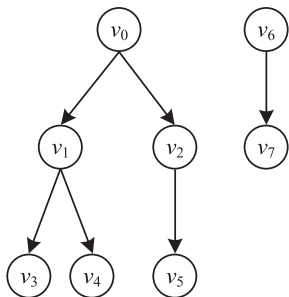


FIGURE 13. Topology inferred by sink node.

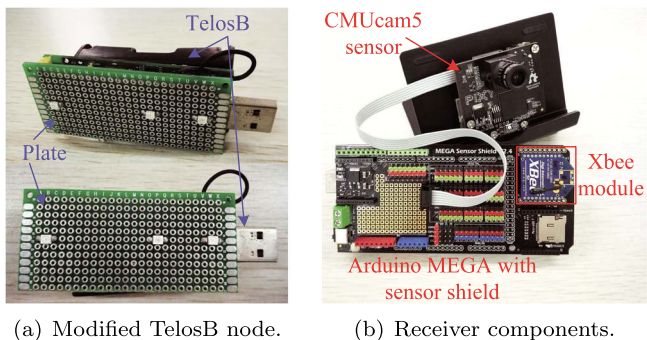


FIGURE 14. LC system testbed.

6. EXPERIMENTAL EVALUATION

6.1. System setup

In the LC system, we employ the TelosB sensor node as the actor node. It is equipped with a TI MSP430 microcontroller, a CC2420 radio chip and a 48-KB program flash memory. We employ a shield plate to cover hardware details so that the camera sensor has good recognition performance. We replace the original three LEDs with three 3.5-mm SMD LEDs. They are further welded onto the shield plate and arranged with heterogeneous spacing. The slightly modified TelosB node is shown in Fig. 14a. Recall that actor nodes shall send a registration frame to the observer node in the registration phase. In our experiment, we program the TelosB node to send radio frames out with a period of 1 second, denoted by T . When TelosB node receives a radio frame from observer node, it turns on corresponding LEDs to represent a binary value of data contained in the radio frame.

The observer node in our LC system is implemented using Arduino Mega 2560 and CMUcam5 [25]. CMUcam5 is an open-source programmable image sensor with an NXP LPC4330 processor and an OV9715 OmniVision camera. The camera supports 1280 by 800 resolution and has a FoV of 75° on horizontal and 47° on vertical. The image sensor applies a hue-based color filtering algorithm to detect objects and then sends only positions to the Arduino (e.g. LED at

$x=100, y=80$). So the CMUcam5 sensor is suitable for the LED detection in our system. As the Arduino receives a series of detected LED positions, it can further perform the process of neighbor identification. To enable the communication between Arduino and TelosB, we adopt an XBee module that supports the IEEE 802.15.4 protocol stack. Various components of the observer node are depicted in Fig. 14b.

Our evaluation is focused on the following metrics:

- System performance under different distances.
- The impact of ambient light intensity on the rate of identification.
- Adaptability of system under different camera viewing angles.
- Robustness of system with different node rotations.
- Average latency of the entire neighbor identification process.
- System's accuracy of distance and angle measurement.

Beside identification latency and measurement accuracy, we test LC in terms of LED *Recognition Ratio* (LRR) and *Neighbor Identification Ratio* (NIR). The former is the ratio between the number of objects recognized as LEDs and the true number of LEDs that appear in the picture. The latter is calculated as the number of neighbors that get identified divided by the total ones in the FoV of camera sensor. In the following section, each experiment consists of 20 tests. Then we provide the average results of all the tests, except for identification latency where we also provide the maximum and minimum values.

6.2. Result analysis

6.2.1. Distance impact on identification

Since the camera sensor is utilized as a receiver of light beams, the distance between the camera sensor and the neighbor node is a key factor affecting system performance. Therefore, we first investigate performance under different distances in terms of LRR and NIR. We put TelosB nodes in the FoV of camera sensor to ensure that all LEDs on the shield plate can be captured. Both of them are placed in a normal indoor illumination condition, about 500 lux. We vary the distance from 20 cm to 80 cm to explore the maximum recognizable distance that LC can achieve. The results are shown in Fig. 15.

It is understandable that LC's ability of LED recognition was influenced by the distance between the camera sensor and TelosB nodes. As the distance increased, LC is hard to distinguish every LED because every LED's region in the picture is small. The camera sensor is likely to recognize only two LEDs in one array pattern instead of three. We can observe that both LRR and NIR drop when the distance is over 60 cm and NIR drops dramatically because incompleteness of recognized LEDs increases the chance of grouping error and thus resulting in a lower NIR. In general, our LC maintains a good identification performance with distance no more than 50 cm. In the following experiment, we fix the distance at 40 cm.

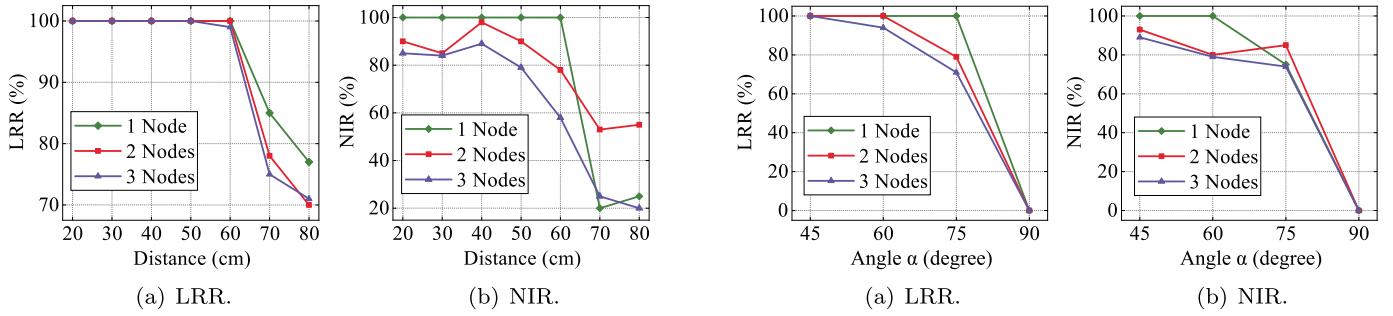


FIGURE 15. Performance under different distances.

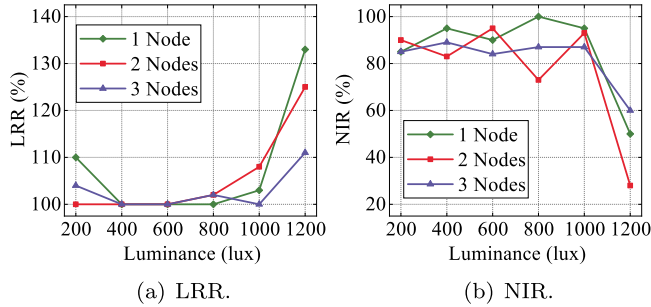


FIGURE 16. Performance under different illuminance.

6.2.2. Impact of ambient light

Since LC transmits identities by light beams, it is of great importance to analyze the impact of ambient light on the performance of LC. Thus, we carry out experiments in a lab under different lighting environments. With fixed node-camera distance, we vary illuminance from 200 lux to 1200 lux, which is monitored by a TSL2561 light sensor near the TelosB node. We keep the camera sensor under default parameter settings. The results in terms of LRR and NIR are shown in Fig. 16.

As LC relies on the recognition of LEDs, a brighter luminance causes a higher camera's recognition error and hence affects the process of neighbor identification. As shown in Fig. 16a, LRR is higher than 100% when light intensity reaches 1200 lux. This fact means that some areas in the picture are also recognized as LEDs and thus the number of LEDs in the picture more than the actual ones. Consequently, LC may not have good identification performance since unreal LEDs affect grouping operation of LED positions, e.g. NIR drops dramatically under 1200 lux in Fig. 16b. Whereas, when ambient light is normal, LC maintains good performance. Although the dim luminance may cause a little high LRR, e.g. 200 lux, NIR still maintains at least 85%. It also implies the robustness of our MI algorithm. In general, LC achieves a good performance in our indoor lighting environment with the illuminance no more than 1000 lux. The factor that most influences performance is the reflected light of the shield plate we employed. Thus, we

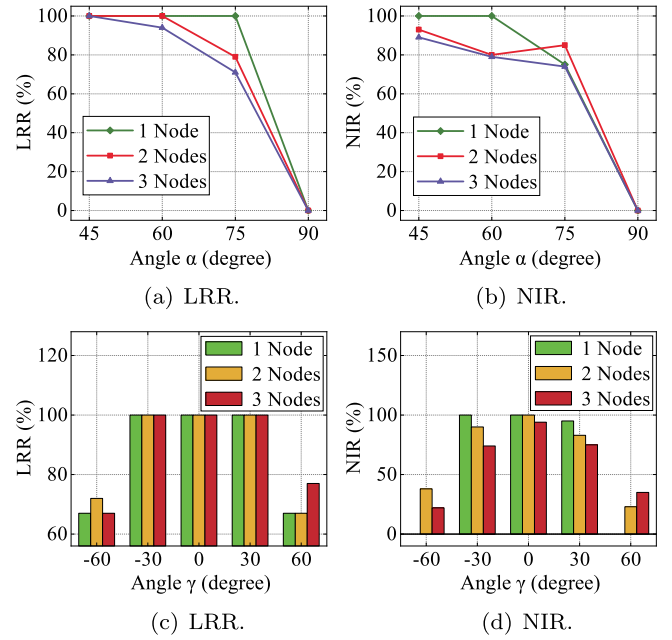


FIGURE 17. Performance under different viewing angles.

recommend using a board with a rough surface to hide node's hardware details.

6.2.3. Performance under viewing angle

In this section, we test the adaptability of LC against different camera viewing angles. We represent viewing angle by two simple angles, α and γ . They denote the pitch angle and yaw angle of a node relative to the camera sensor, respectively. These two angles are shown in Fig. 18 and Fig. 19. With fixed distance and illumination intensity, we vary the angle α between $[0^\circ, 90^\circ]$ and γ between $[-60^\circ, 60^\circ]$ to emulate all possible realistic scenarios. For example, if a node faces the camera sensor perpendicularly, the viewing angle can be represented as $\alpha = 0^\circ$ and $\gamma = 0^\circ$. If the node deflects to the left, then the value of γ is negative. When we test the performance under different α , we keep $\gamma = 0^\circ$. Similarly, the angle α is kept at 0° while measuring the maximum deflection angle of node. The results in terms of LRR and NIR are shown in Fig. 17. Although the performance under α between $[0^\circ, 45^\circ]$ is not provided, LC still maintains good performance.

Figure 17 shows that LC's performance degrades as the viewing angle increased. A larger viewing angle leads to a more weakened light received by camera sensor that in turn affects the process of LED recognition. To be specific, LC fails to detect the dim LED in the picture because the camera sensor we employed detects objects by color hue. Then the partial detected LEDs cause grouping incorrectness and hence affect the process of neighbor identification. Consequently, we can observe both LRR and NIR reduce when angle α or γ increases.

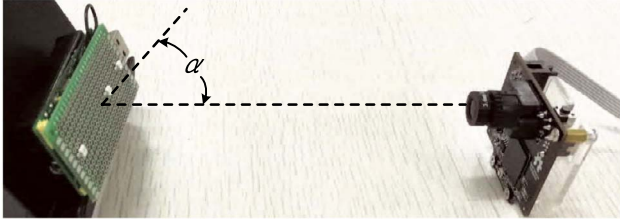
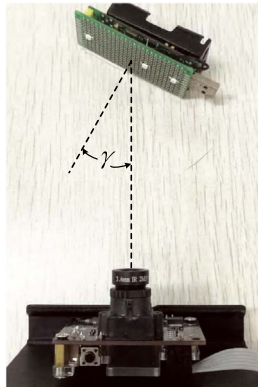
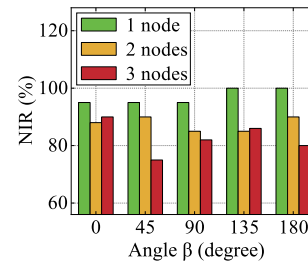
FIGURE 18. Pitch angle α .FIGURE 19. Yaw angle γ .FIGURE 20. Roll angle β .

FIGURE 21. Performance under varying rotations.

Overall, LC maintains a rather good performance with α no more than 75° and γ between $[-30^\circ, 30^\circ]$. Such a wild viewing angle makes LC have good adaptability in the actual scenarios.

6.2.4. Performance under node rotation

In addition to the adaptability, we next test the robustness of LC under different node rotations, i.e. roll angles as illustrated in Fig. 20. Likewise, we fix the camera sensor at a 40-cm distance and illumination intensity at 500 lux. Then we vary node's roll angles, denoted by β , from 0° to 180° . When the node faces a camera sensor horizontally, the angle β equals to 0° . If the node is upside down, then $\beta = 180^\circ$. Throughout the experiment, we keep nodes facing forward to the camera sensor all the time to ensure that all LEDs can be captured.

As we measured in section 6.2.1. The performance in terms of LRR maintains 100% consistently since node-camera distance, ambient light intensity and viewing angles are all in good condition. Thus, we provide only evaluation results in terms of NIR in Fig. 21. When the roll angle varies, NIR changes slightly. This observation indicates the stability and robustness of LC in most roll angle ranges. Although performance degrades when there are more than one node, LC still maintains NIR of about 75%. This result benefits from the design of the LED array pattern since it serves as a criterion for grouping LED positions correctly.

6.2.5. Average identification latency

We finally evaluate the identification latency cost by LC. Identification latency is defined as the time span from observer node receiving registration frames till all neighbor nodes get identified. It mainly consists of two parts of time: the waiting time for registration and the processing time of hardware. Recall that each actor node is configured to send registration frames to the observer node with a period T , i.e. 1 second. So, in our experiment, the waiting time of registration frame is set to a value equal to period T , which ensures that registration frames can be received while keeping the waiting time as short as possible. The second one mainly depends on the amount of detected LED positions. Thus, we investigate identification latency under a varying number of nodes.

As we would expect, Fig. 22 shows that the total time increases with the number of nodes. The more nodes appear in the FoV of camera sensor, the more LEDs detected, i.e. the more LED positions exist in the set S . Thus, the observer node needs much time to determine which three LED positions come from the same node. We also observe that the average identification latency of each node decreases as the increment of node's number. For example, the average latency is 1087 ms when there are three nodes, less than 1342 ms when there are two nodes. Based on this, we can conclude that LC is

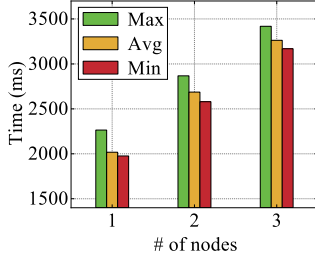


FIGURE 22. Identification latency.

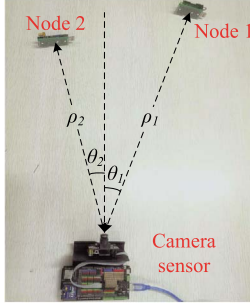


FIGURE 23. An example of measuring relative position.

computationally efficient for the situation where one node often has multiple neighbor nodes.

6.2.6. Measurement accuracy

In our LC system, an observer node can calculate the relative distances and angles of actor nodes by exploiting the image information captured by the camera. In this section, we investigate the accuracy of distance and angle measurement. We put the TelosB node and the camera on a horizontal desktop without any obstacle between them. The node keeps facing forward to the camera but is placed at different positions. The ambient light intensity is controlled in a constant state. Figure 23 shows an example in which two Telosb nodes are placed in the FoV of camera. Their distances relative to the camera are denoted by ρ_1 and ρ_2 , respectively. The relative angles are denoted by θ_1 and θ_2 , respectively. We evaluate the measurement accuracy by comparing the true ρ and θ with the calculated results of LC at different positions.

We divide camera's fan-shaped coverage area into multiple rectangles and each rectangle has a width of 5 cm and a height of 10 cm. The vertices of these rectangles are referred to as candidate positions. Thus, we get 42 candidate positions in the FoV of camera as depicted in Fig. 24. In these 42 candidate positions, 10 test positions are selected randomly where we place a TelosB node and perform the measurement of distance and angle. At each test position, we do 20 calculations and then provide the average errors. The experimental results are shown in Fig. 25.

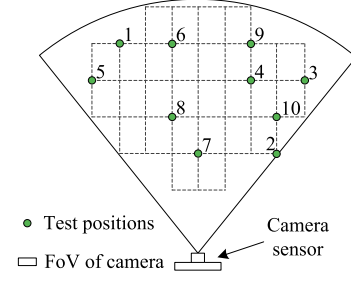


FIGURE 24. Select 10 test positions from 42 candidate positions.

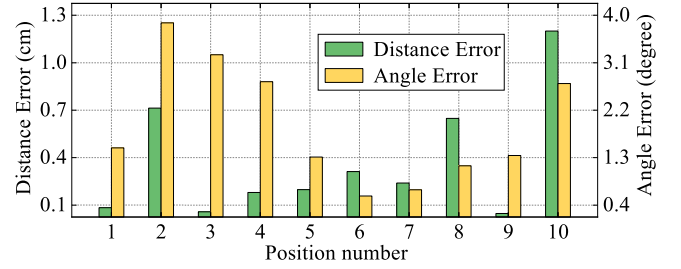


FIGURE 25. Accuracy of distance and angle measurement.

TABLE 3 Comparison of measurement error.

System	Distance Error (mm)		Angle Error (°)	
	Avg.	S.D.	Avg.	S.D.
LC	3.70	3.58	1.67	10.78
LISTEN [6]	28.82	12.08	0.42	0.18

As can be seen from Fig. 25, both distance error and angle error keep low at most test positions. One reason that can account for the high error is the image distortion. The image distortion makes the pixel measurement of LEDs at the edge of picture very different from the real value and further affects the calculation of relative distances and angles. Two obvious examples are the measurement results at position 2 and 10. Although this situation exists, the average errors on distance and angle measurement are 0.37 cm and 1.67°, respectively. Then the relative average errors are 0.89% and 11.08%, respectively. We also provide a comparison with the results in [6] in terms of average (Avg.) and standard deviation (S.D.) error of distance and angle measurement in Table 3. In general, the accurate relative measurement can be achieved and it provides a guarantee for the accurate neighbor identification.

7. SIMULATIONS

In this section, we perform extensive simulations to verify the feasibility of topology inference by such neighbor identification process. Moreover, we study how the number of nodes affects topology construction in a given size region. Also, the maximum number of identification required to deduce topology is investigated.

7.1. Simulation settings

We first assume that each node has a wireless communication radius of 20 m. Two nodes with a distance less than this threshold can establish a communication link between each other and transmit/receive neighbor identification information. View range and FoV of the equipped camera sensor are defined as 15 m and 90° , respectively. If a node v_j is covered by the fan-shape area of node v_i , then node v_j is identified by node v_i .

The simulations are performed within two different sized regions: *small region* (SR) and *large region* (LR). The SR is a 60 m by 60 m square area and the LR is a 130 m by 130 m square. In two different regions, we both generate a sink node and several common nodes with random camera orientations while their locations satisfy a specified distribution. In the following simulations, we are mainly concerned about two common distribution pattern: *uniform distribution* (UD) and *normal distribution* (ND). For a particular distribution, we vary the total number of nodes, denoted by ‘# of nodes’, from 5 to 120 with the increment of 5. In each setting, the average result of 150 independent simulations is calculated.

7.2. Topology similarity

After all nodes are generated, we simulate the data aggregation process in which neighbor identification information is aggregated from each node to the same destination, i.e. sink node. With identification information collected, the sink node constructs a directed graph, i.e. topology, though a breadth-first search. Obviously, if there is no communication path between node v_k and sink node due to too few relay nodes, then the identification information of node v_k will not be collected by sink node. That is, node v_k does not appear in the directed graph built by sink node. Therefore, we evaluate the impact of node number on topology similarity. Topology similarity is defined as the ratio between the number of identified sensor nodes and the total number of nodes in the simulation area [28, 29].

The relationship between topology similarity and the number of nodes is depicted in Fig. 26. Intuitively, the topology similarity increases with the number of nodes. In a given sized region, the network has a great node density as the number of nodes increases. Thus, there is a great likelihood for nodes to identify each other. This phenomenon is especially obvious in SR. As shown in Fig. 26a, topology similarity in SR increases significantly since it is easier to achieve high node density

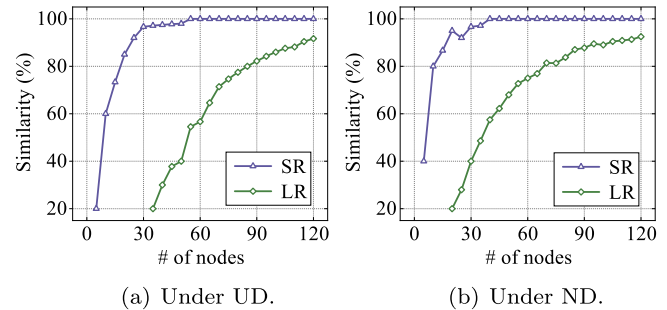


FIGURE 26. Topology similarity in two regions under both UD and ND.

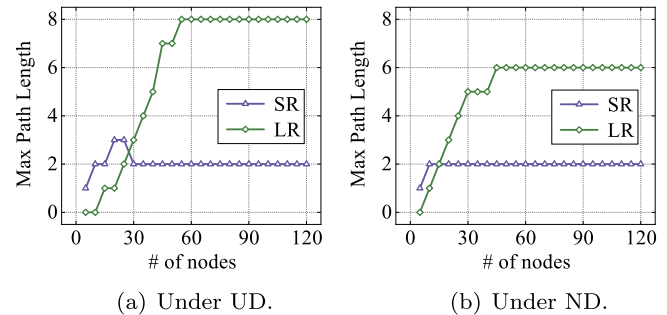


FIGURE 27. Max path length in two regions under both UD and ND.

compared with the one in LR. Although the topology similarity in LR increases slowly, it can achieve about 91% when there are 120 nodes deployed in the network. Therefore, both evaluations in SR and LR validate the feasibility of topology inference through the neighbor identification process.

We also study the topology similarity when nodes’ locations satisfy ND since it is closer to practical deployment. The simulation results are illustrated in Fig. 26b. Compared with Fig. 26a, topology similarity under ND shows similar variation characteristics. Furthermore, it shows a higher value in LR. For example, when there are 60 nodes in the network, topology similarity under ND is 75%, which is higher than 56% under UD. This implies that a high topology similarity can be achieved in practical large-region node deployment.

Although Fig. 26 does not give the variation trend of topology similarity of LR under UD and ND when the number of nodes exceeds 120, they both maintained above 90% and close to 100%. When there are 200 nodes in the network, both two green curves reach 97%.

7.3. Maximum number of identification

In our simulations, the directed graph is constructed though the breadth-first search, which represents the worst case of practical topology inference. Specifically, it takes the most time to complete the process of topology inference. The time it takes is largely related to the number of executions of breadth-

first search. Thus, we study the maximum path length of the constructed directed graph under the same simulation settings as before.

Figure 27a shows that the maximum path length of a constructed directed graph in SR and LR under UD is 2 and 8, respectively. That is if there are 120 nodes deployed in LR, a topology containing 91% nodes can be concluded with no more than eight neighbor identification processes. For the case of ND, we find that the maximum path length has a decrement in LR, as shown in Fig. 27b. The topology inference can be accomplished within six neighbor identification processes. Both investigations suggest that it is efficient and fast to infer topology through such neighbor identification process.

8. RELATED WORK

Neighbor Discovery. As some previous studies illustrated, neighbor discovery has attracted a lot of research works [3, 30–33]. Cai *et al.* present a randomized 2-way neighbor discovery algorithm to solve the neighbor discovery problem where nodes are equipped with directional antennas [34]. Chen *et al.* also study the oblivious neighbor discovery problem in which the devices have directional antennas and design a protocol to guarantee the order-minimal worst-case discovery delay [35]. Cai *et al.* propose a quorum-based neighbor discovery algorithm to decrease the impact of collisions caused by simultaneous communication between multiple nodes pairs [36].

Localization. Prior researches about sensor localization are based on wireless signals [37]. Wu *et al.* construct an RSS map of a floor plan to achieve indoor localization with off-the-shelf WiFi infrastructure and mobile phones [14]. Chen *et al.* propose an approach (AutoFi) to automatically calibrate the localization profile when environment changes [15].

Whereas, another kind of researches devote to localize sensor nodes by exploiting image information [38]. Barton-Sweeney *et al.* propose an algorithm to localize a large number of sensor nodes by exchanging information among the nodes equipped with CMOS cameras [39]. Yang *et al.* present an accurate indoor localization system (Flash-Loc) in which surveillance cameras are used to distinguish each person [40].

Visible Light Communication. Advances in VLC have attracted many interesting researches in recent years [41, 42]. Hu *et al.* present an LED-to-camera communication system leveraging tri-LED's ability to provide a variety of colors [43]. Similarly, Yang *et al.* present an LED-to-Camera VLC system in which three lights working on the same frequency are utilized to create different brightness levels [44].

Another application of visible light is indoor positioning [45–47]. Li *et al.* fabricate an anchor that can take on various color hues as the observation position changes [48]. They derive a model that characterizes the relationship of direction and chips' color to realize 3D localization. Similarly, Tian *et al.* fabricate a lamp cover through which the light projects

a specific color pattern on the floor, then augmenting IMU's tracking accuracy [49].

9. CONCLUSION

In this paper, we present LC, a novel image-based neighbor identification system. Compared with existing methods, LC provides an effective and fast performance, mainly because it realizes neighbor identification relying on the image that has more dimensions than wireless signals. To achieve the correct identity expression and extraction, LCP is proposed. LCP also provides a method of measuring neighbors' relative positions. Using the self-built testbed, we evaluate adaptability and robustness of LC under different environmental conditions. Besides, the feasibility and efficiency of topology inference through such neighbor identification process are validated by extensive simulations.

10. FUNDING

National Natural Science Foundation of China (61473109); Zhejiang Major Science and Technology Programme (2018C04012); National Natural Science Foundation of China (61572164 and 61877015); General Research Foundation of the Education Department of Zhejiang Province (Y201840731) Graduate Scientific Research Foundation of Hangzhou Dianzi University (CXJJ2018053).

REFERENCES

- [1] Zhang, J., Li, Z. and Tang, S. (2016) Value of information aware opportunistic duty cycling in solar harvesting sensor networks. *THI*, 12, 348–360. doi: [10.1109/THI.2015.2508745](https://doi.org/10.1109/THI.2015.2508745).
- [2] Zhang, X., Chen, H., Lin, K., Wang, Z., Yu, J. and Shi, L. (2019) Rmts: a robust clock synchronization scheme for wireless sensor networks. *JNCA*, 135, 1–10. doi: [10.1016/j.jnca.2019.02.028](https://doi.org/10.1016/j.jnca.2019.02.028).
- [3] Meng, T., Wu, F. and Chen, G. (2016) Code-based neighbor discovery protocols in mobile wireless networks. *TON*, 24, 806–819. doi: [10.1109/TNET.2015.2388534](https://doi.org/10.1109/TNET.2015.2388534).
- [4] Sun, W., Yang, Z., Zhang, X. and Liu, Y. (2014) Energy-efficient neighbor discovery in mobile ad hoc and wireless sensor networks: a survey. *IEEE Commun. Surv. Tut.*, 16, 1448–1459. doi: [10.1109/SURV.2013.012414.00164](https://doi.org/10.1109/SURV.2013.012414.00164).
- [5] Akyildiz, I.F., Melodia, T. and Chowdhury, K.R. (2007) A survey on wireless multimedia sensor networks. *Comput. Netw.*, 51, 921–960. doi: [10.1016/j.comnet.2006.10.002](https://doi.org/10.1016/j.comnet.2006.10.002).
- [6] He, Y., Shen, X., Liu, Y., Mo, L., and Dai, G. (2010) Listen: Non-Interactive Localization in Wireless Camera Sensor Networks. In *Proc. RTSS 10, San Diego, CA, 30 November–3 December*, pp. 205–214. IEEE, New York. DOI: [10.1109/RTSS.2010.15](https://doi.org/10.1109/RTSS.2010.15).
- [7] Danakis, C., Afgani, M., Povey, G., Underwood, I., and Haas, H. (2012) Using a CMOS Camera Sensor for Visible Light Communication. In *Proc. GC Wkshps 12, Anaheim, CA, 3–7 December*, pp. 1244–1248. IEEE, New York. DOI: [10.1109/GLOCOMW.2012.6477759](https://doi.org/10.1109/GLOCOMW.2012.6477759).

- [8] Yang, Y., Hao, J. and Luo, J. (2017) Ceilingtalk: lightweight indoor broadcast through LED-camera communication. *TMC*, 16, 3308–3319. doi: [10.1109/TMC.2017.2694834](https://doi.org/10.1109/TMC.2017.2694834).
- [9] Khan, A.A., Rehmani, M.H. and Saleem, Y. (2015) Neighbor discovery in traditional wireless networks and cognitive radio networks: basics, taxonomy, challenges and future research directions. *JNCA*, 52, 173–190. doi: [10.1016/j.jnca.2015.03.003](https://doi.org/10.1016/j.jnca.2015.03.003).
- [10] Wang, K., Mao, X. and Liu, Y. (2015) Blinddate: a neighbor discovery protocol. *TPDS*, 26, 949–959. doi: [10.1109/ICPP.2013.21](https://doi.org/10.1109/ICPP.2013.21).
- [11] Sun, W., Yang, Z., Wang, K., and Liu, Y. (2014) Hello: A Generic Flexible Protocol for Neighbor Discovery. In *Proc. INFOCOM 14, Toronto, ON, 27 April–2 May, pp. 540–548*. IEEE, New York. DOI: [10.1109/INFOCOM.2014.6847978](https://doi.org/10.1109/INFOCOM.2014.6847978).
- [12] Chen, L., Fan, R., Bian, K., Gerla, M., Wang, T., and Li, X. (2015) On Heterogeneous Neighbor Discovery in Wireless Sensor Networks. In *Proc. INFOCOM 15, Kowloon, Hong Kong, 26 April–1 May, pp. 693–701*. IEEE, New York. DOI: [10.1109/INFOCOM.2015.7218438](https://doi.org/10.1109/INFOCOM.2015.7218438).
- [13] Wang, J., Ghosh, R.K. and Das, S.K. (2010) A survey on sensor localization. *JCTA*, 8, 2–11. doi: [10.1007/s11768-010-9187-7](https://doi.org/10.1007/s11768-010-9187-7).
- [14] Wu, C., Yang, Z. and Liu, Y. (2015) Smartphones based crowdsourcing for indoor localization. *TMC*, 14, 444–457. doi: [10.1109/TMC.2014.2320254](https://doi.org/10.1109/TMC.2014.2320254).
- [15] Chen, X., Ma, C., Allegue, M., and Liu, X. (2017) Taming the Inconsistency of Wi-Fi Fingerprints for Device-Free Passive Indoor Localization. In *Proc. INFOCOM 17, Atlanta, GA, 1–4 May, pp. 1–9*. IEEE, New York. DOI: [10.1109/INFOCOM.2017.8057185](https://doi.org/10.1109/INFOCOM.2017.8057185).
- [16] Assaf, A.E., Zaidi, S., Affes, S. and Kandil, N. (2016) Low-cost localization for multihop heterogeneous wireless sensor networks. *IEEE T. Wirel. Commun.*, 15, 472–484. doi: [10.1109/TWC.2015.2475255](https://doi.org/10.1109/TWC.2015.2475255).
- [17] Li, H. and Xu, Z. (2018) Self-Adaptive Neighbor Discovery in Mobile Ad Hoc Networks With Directional Antennas. In *Proc. ICC Workshops 18, Kansas City, MO, 20–24 May, pp. 1–6*. IEEE, New York. DOI: [10.1109/ISTMWC.2007.4299291](https://doi.org/10.1109/ISTMWC.2007.4299291).
- [18] Kindt, P.H., Saur, M., Balszun, M. and Chakraborty, S. (2018) Neighbor discovery latency in ble-like protocols. *TMC*, 17, 617–631. doi: [10.1109/TMC.2017.2737008](https://doi.org/10.1109/TMC.2017.2737008).
- [19] Shieh, C.-S., Sai, V.-O., Lin, Y.-C., Lee, T.-F., Nguyen, T.-T., and Le, Q.-D. (2016) Improved Node Localization for WSN Using Heuristic Optimization Approaches. In *Proc. NaNA 16, Hakodate, Japan, 23–25 July, pp. 95–98*. IEEE, New York. DOI: [10.1109/NaNA.2016.58](https://doi.org/10.1109/NaNA.2016.58).
- [20] Han, G., Jiang, J., Zhang, C., Duong, T.Q., Guizani, M. and Karagiannidis, G.K. (2016) A survey on mobile anchor node assisted localization in wireless sensor networks. *IEEE Commun. Surv. Tut.*, 18, 2220–2243. doi: [10.1109/COMST.2016.2544751](https://doi.org/10.1109/COMST.2016.2544751).
- [21] Zhang, J., Zheng, S., Zhang, T., Wang, M. and Li, Z. (2019) Charge-aware duty cycling methods for wireless systems under energy harvesting heterogeneity. *TOSN* 16, 1–23. doi: [10.1145/3372800](https://doi.org/10.1145/3372800).
- [22] Wu, Y., Wang, Y., Hu, W. and Cao, G. (2016) Smartphoto: a resource-aware crowdsourcing approach for image sensing with smartphones. *TMC*, 15, 1249–1263. doi: [10.1145/2632951.2632979](https://doi.org/10.1145/2632951.2632979).
- [23] Lee, H.-Y., Lin, H.-M., Wei, Y.-L., Wu, H.-I., Tsai, H.-M., and Lin, K. C.-J. (2015) Rollinglight: Enabling Line-of-Sight Light-to-Camera Communications. In *Proc. MobiSys 15, Florence, Italy, 18–22 May, pp. 167–180*. ACM, New York. DOI: [10.1145/2742647.2742651](https://doi.org/10.1145/2742647.2742651).
- [24] Hao, J., Yang, Y., and Luo, J. (2016) Ceilingcast: Energy Efficient and Location-Bound Broadcast Through LED-Camera Communication. In *Proc. INFOCOM 16, San Francisco, CA, 10–15 April, pp. 1–9*. IEEE, New York. DOI: [10.1109/INFOCOM.2016.7524511](https://doi.org/10.1109/INFOCOM.2016.7524511).
- [25] Jfrench (2018) *Pixy (cmucam5) documentation*. <https://docs.pixycam.com/wiki/doku.php?id=wiki:v1:start>. (accessed July 7, 2018).
- [26] Alexander, L. W. L., Isa, K., Kadir, H. A., and Ambar, R. (2019) Development of an Autonomous Underwater Vehicle for Target Acquisition. In *Proc. NUSYS 18, Singapore, 9 February, pp. 65–78*. Springer, Singapore. DOI: [10.1007/978-981-13-3708-6_7](https://doi.org/10.1007/978-981-13-3708-6_7).
- [27] He, Y., Liu, Y., Shen, X., Mo, L., and Dai, G. (2013) Noninteractive localization of wireless camera sensors with mobile beacon. *TMC*, 12, 333–345. DOI: [10.1109/TMC.2011.278](https://doi.org/10.1109/TMC.2011.278).
- [28] Tao, Z., Cai, W., and Li, Y. (2007) Using End-to-End Data to Infer Sensor Network Topology. In *Proc. ISSPIT 07, Giza, Egypt, 15–18 December, pp. 504–508*. IEEE, New York. DOI: [10.1109/ISSPIT.2007.4458012](https://doi.org/10.1109/ISSPIT.2007.4458012).
- [29] Tao, Z., Cai, W. D., and Li, Y. J. (2007) Mvida: A Sensor Network Topology Inference Algorithm. In *Proceedings of CIS 07, Harbin, China, 15–19 December, pp. 451–455*. IEEE, New York. DOI: [10.1109/CIS.2007.44](https://doi.org/10.1109/CIS.2007.44).
- [30] Zhang, R. and Zhang, Y. (2010) Wormhole-Resilient Secure Neighbor Discovery in Underwater Acoustic Networks. In *Proc. INFOCOM 10, San Diego, CA, 15–19 March, pp. 1–9*. IEEE, New York. DOI: [10.1109/INFOCOM.2010.5462093](https://doi.org/10.1109/INFOCOM.2010.5462093).
- [31] Qiu, Y., Li, S., Xu, X., and Li, Z. (2016) Talk More Listen Less: Energy-Efficient Neighbor Discovery in Wireless Sensor Networks. *Proc. INFOCOM 16, San Francisco, CA, 10–15 April, pp. 1–9*. IEEE, New York. DOI: [10.1109/INFOCOM.2016.7524336](https://doi.org/10.1109/INFOCOM.2016.7524336).
- [32] Zhang, R., Zhang, Y., and Huang, X. (2011) JR-SND: Jamming-Resilient Secure Neighbor Discovery in Mobile Ad Hoc Networks. *Proc. ICDCS 11, Minneapolis, MN, 20–24 June, pp. 529–538*. IEEE, New York. DOI: [10.1109/ICDCS.2011.53](https://doi.org/10.1109/ICDCS.2011.53).
- [33] Kandhalu, A., Lakshmanan, K., and Rajkumar, R. (2010) U-Connect: A Low-Latency Energy-Efficient Asynchronous Neighbor Discovery Protocol. In *Proc. IPSN 10, Stockholm Sweden, 12–16 April, pp. 350–361*. ACM, New York. DOI: [10.1145/1791212.1791253](https://doi.org/10.1145/1791212.1791253).
- [34] Cai, H. and Wolf, T. (2015) On 2-Way Neighbor Discovery in Wireless Networks With Directional Antennas. In *Proc. INFOCOM 15, Kowloon, Hong Kong, 26 April–1 May, pp. 702–710*. IEEE, New York. DOI: [10.1109/INFOCOM.2015.7218439](https://doi.org/10.1109/INFOCOM.2015.7218439).
- [35] Chen, L., Li, Y., and Vasilakos, A. V. (2016) Oblivious Neighbor Discovery for Wireless Devices With Directional Antennas. In *Proc. INFOCOM 16, San Francisco, CA, 10–15 April, pp. 1–9*. IEEE, New York. DOI: [10.1109/INFOCOM.2016.7524570](https://doi.org/10.1109/INFOCOM.2016.7524570).
- [36] Cai, H. and Wolf, T. (2018) Self-Adapting Quorum-Based Neighbor Discovery in Wireless Sensor Networks. In *Proc. INFOCOM 18, Honolulu, HI, 15–19 April, pp. 324–332*. IEEE, New York, NY. DOI: [10.1109/INFOCOM.2018.8486268](https://doi.org/10.1109/INFOCOM.2018.8486268).

- [37] Großwindhager, B., Rath, M., Kulmer, J., Bakr, M. S., Boano, C. A., Witrisal, K., and Römer, K. (2018) Salma: UWB-Based Single-Anchor Localization System Using Multipath Assistance. In *Proc. SenSys 18, Shenzhen, China, 4–7 November*, pp. 132–144. ACM, New York. DOI: [10.1145/3274783.3274844](https://doi.org/10.1145/3274783.3274844).
- [38] Diamond, D., O'Connor, N. E., Smeaton, A. F., Beirne, S., Corcoran, B., Kelly, P., Lau, K. T., and Shepherd, R. (2007) Sensor Node Localisation Using a Stereo Camera Rig. In *Proc. EmNets 07, Cork, Ireland, 25–26 June*, pp. 43–47. ACM, New York. DOI: [10.1145/1278972.1278983](https://doi.org/10.1145/1278972.1278983).
- [39] Barton-Sweeney, A., Lymberopoulos, D., and Sawides, A. (2006) Sensor Localization and Camera Calibration in Distributed Camera Sensor Networks. In *Proc. ICBCNS 06, San Jose, CA, 1–5 October*, pp. 1–10. IEEE, New York. DOI: [10.1109/BROADNETS.2006.4374301](https://doi.org/10.1109/BROADNETS.2006.4374301).
- [40] Yang, F., Zhai, Q., Chen, G., Champion, A. C., Zhu, J., and Xuan, D. (2016) Flash-loc: Flashing Mobile Phones for Accurate Indoor Localization. In *Proc. INFOCOM 16, San Francisco, CA, 10–15 April*, pp. 1–9. IEEE, New York. DOI: [10.1109/INFOCOM.2016.7524391](https://doi.org/10.1109/INFOCOM.2016.7524391).
- [41] Li, T., An, C., Tian, Z., Campbell, A. T., and Zhou, X. (2015) Human Sensing Using Visible Light Communication. In *Proc. MobiCom 15, Paris, France, 7–11 September*, pp. 331–344. ACM, New York. DOI: [10.1145/2789168.2790110](https://doi.org/10.1145/2789168.2790110).
- [42] Schmid, S., Corbellini, G., Mangold, S., and Gross, T. R. (2013) LED-to-LED Visible Light Communication Networks. In *Proc. MobiHoc 13, Bangalore, India, 29 July–1 August*, pp. 1–10. ACM, New York. DOI: [10.1145/2491288.2491293](https://doi.org/10.1145/2491288.2491293).
- [43] Hu, P., Pathak, P. H., Feng, X., Fu, H., and Mohapatra, P. (2015) Colorbars: Increasing Data Rate of LED-to-Camera Communication Using Color Shift Keying. In *Proc. CoNEXT 15, Heidelberg, Germany, 1–4 December*, pp. 12:1–12:13. ACM, New York. DOI: [10.1145/2716281.2836097](https://doi.org/10.1145/2716281.2836097).
- [44] Yang, Y., Nie, J., and Luo, J. (2017) Reflexcode: Coding With Superposed Reflection Light for LED-Camera Communication. In *Proc. MobiCom 17, Snowbird, Utah, 16–20 October*, pp. 193–205. ACM, New York. DOI: [10.1145/3117811.3124770](https://doi.org/10.1145/3117811.3124770).
- [45] Zhang, C. and Zhang, X. (2016) Litell: Robust Indoor Localization Using Unmodified Light Fixtures. In *Proc. MobiCom 16, New York, NY, 3–7 October*, pp. 230–242. ACM, New York. DOI: [10.1145/2973750.2973767](https://doi.org/10.1145/2973750.2973767).
- [46] Zhang, C. and Zhang, X. (2017) Pulsar: Towards Ubiquitous Visible Light Localization. In *Proc. MobiCom 17, Snowbird, Utah, 16–20 October*, pp. 208–221. ACM, New York. DOI: [10.1145/3117811.3117821](https://doi.org/10.1145/3117811.3117821).
- [47] Liu, S. and He, T. (2017) Smartlight: Light-Weight 3d Indoor Localization Using a Single LED Lamp. In *Proc. SenSys 17, Delft, Netherlands, 6–8 November*, pp. 11:1–11:14. ACM, New York. DOI: [10.1145/3131672.3131677](https://doi.org/10.1145/3131672.3131677).
- [48] Li, L., Xie, P., and Wang, J. (2018) Rainbowlight: Towards Low Cost Ambient Light Positioning With Mobile Phones. In *Proc. MobiCom 18, New Delhi, India, 29 October–2 November*, pp. 445–457. ACM, New York. DOI: [10.1145/3241539.3241545](https://doi.org/10.1145/3241539.3241545).
- [49] Tian, Z., Wei, Y.-L., Chang, W.-N., Xiong, X., Zheng, C., Tsai, H.-M., Lin, K. C.-J., and Zhou, X. (2018) Augmenting Indoor Inertial Tracking With Polarized Light. In *Proc. MobiSys 18, Munich, Germany, 10–15 June*, pp. 362–375. ACM, New York. DOI: [10.1145/3210240.3210340](https://doi.org/10.1145/3210240.3210340).